Published in final edited form as:
Invest Ophthalmol Vis Sci. 2007 June ; 48(6): 2576–2588.

Horizontal Rectus Muscle Anatomy in Naturally and Artificially Strabismic Monkeys

Anita Narasimhan[1,2], **Lawrence Tychsen**[3,4,5], **Vadims Poukens**[1], and **Joseph L. Demer**[1,2,6,7]

1*Department of Ophthalmology, University of California, Los Angeles, California*

2*Bioengineering Interdepartmental Program, University of California, Los Angeles, California*

3*Department of Ophthalmology and Visual Sciences, Washington University School of Medicine, St. Louis, Missouri*

4*Department of Anatomy and Neurobiology, Washington University School of Medicine, St. Louis, Missouri*

5*Department of Pediatrics, Washington University School of Medicine, St. Louis, Missouri*

6*Department of Neuroscience and Neurology, University of California, Los Angeles, California*

7*Neuroscience Interdepartmental Program, University of California, Los Angeles, California*

Abstract

Purpose—Structural abnormalities of extraocular muscles (EOMs) or their pulleys are associated with some forms of human strabismus. This experiment was conducted to investigate whether such abnormalities are associated with artificial or naturally occurring strabismus in monkeys.

Methods—Binocular alignment and grating visual acuities were determined in 10 monkeys representing various species using search coil recording and direct observations. Four animals were orthotropic, two had naturally occurring “A”-pattern esotropia, two had concomitant and one had “V”-pattern esotropia artificially induced by alternating or unilateral occlusion in infancy, and one had “A”-pattern exotropia artificially induced by prism wear. After euthanasia, 16 orbits were examined by high-resolution magnetic resonance imaging (MRI) in the quasicoronal plane. Paths and sizes of horizontal rectus EOMs were analyzed quantitatively in a standardized coordinate system. Whole orbits were then serially sectioned en bloc in the quasicoronal plane, stained for connective tissue, and compared with MRI. Nerve and EOM features were analyzed quantitatively.

Results—Quantitative analysis of MRI revealed no significant differences in horizontal rectus EOM sizes or paths among orthotropic or naturally or artificially strabismic monkeys. Histologic examination demonstrated no differences in EOM size, structure, or innervation among the three groups, and no differences in connective tissues in the pulley system. The accessory lateral rectus (ALR) EOM was present in all specimens, but was small, inconsistently located, and sparsely innervated. Characteristics of the ALR did not correlate with strabismus.

Conclusions—Major structural abnormalities of horizontal rectus EOMs and associated pulleys are unrelated to natural or artificial horizontal strabismus in the monkeys studied. The ALR is unlikely to contribute to horizontal strabismus in primates. However, these findings do not exclude a possible role of pulley abnormalities in disorders such as cyclovertical strabismus.

Before the development of quantitative models of extraocular biomechanics,[1–3] it was believed sufficient to describe orbital anatomy by cadaveric measurements of extraocular

Corresponding author: Joseph L. Demer, Jules Stein Eye Institute, 100 Stein Plaza, UCLA, Los Angeles, CA 90095-7002; jld@ucla.edu
Disclosure: **A. Narasimhan**, None; **L. Tychsen**, None; **V. Poukens**, None; **J.L. Demer**, None

muscle (EOM) origins and insertions. These descriptions inform classic concepts of EOM actions and most current strabismus surgery. Attempts to calculate binocular alignment from these first principles then made it obvious that EOM paths, the gaze dependence of paths, and the supporting orbital tissues, were critical to ocular motility. Radiography in monkeys[4] and humans[5] subsequently suggested that rectus EOM bellies have stable paths relative to the orbit, despite gaze changes. Miller first used magnetic resonance imaging (MRI) to demonstrate the stability of rectus EOM belly paths in humans and initiated the notion that pulleys influence rectus EOM paths.[6]

It has subsequently emerged that the rectus and inferior oblique EOMs of humans and monkeys do indeed have highly structured soft pulleys that regulate EOM pulling directions.[7–10] The pulleys act as functional origins of the rectus EOMs.[11] Rectus EOMs travel through their respective pulleys, which imply that the pulleys must lie along the EOM paths. Many cases of human incomitant cyclovertical strabismus are associated with displacement of one or more rectus EOM pulleys. “A” and “V” patterns of incomitance in strabismic patients consistently match those predicted by computational simulation based on measured pulley locations, suggesting that pulley heterotopy *caused* the strabismus.[12,13] Extreme pulley heterotopy is associated with esotropia and hypotropia in axial high myopia, the “heavy-eye syndrome.”[14–16]

The most common forms of human strabismus are horizontal, concomitant eso- and exotropia. Concomitant strabismus means that the degree of misalignment is the same regardless of horizontal gaze direction, although “A” and “V” patterns of variation with vertical gaze are typically associated with the most common forms in humans.[14] Infantile esotropia is particularly prevalent in humans and is often associated with a “V” pattern, in which the esodeviation increases in downward gaze.[17] The possible contribution of pulley abnormalities to human concomitant strabismus is unknown, as it is difficult to study in children who typically cannot cooperate for adequate magnetic resonance imaging (MRI). Even if rectus pulleys were found to be abnormal in humans with horizontal concomitant strabismus, it would be impossible to know whether the abnormalities were the causes or effects of the strabismus.

A primate model offers a solution to the conundrum. The visual and oculomotor systems of monkeys are considered good models of the human because of peripheral orbital and neuroanatomic similarities.[18–20] Infantile esotropia occurs naturally in monkeys, and strabismus can be induced artificially by optical means or lid suturing. Investigation in monkeys also affords opportunity to study the accessory lateral rectus (ALR) muscle, which occurs variably in some species, and has been said to be a factor in the prevalence of natural simian esotropia.[21] The present study used MRI and serial histology to determine whether any abnormalities of the horizontal rectus EOMs or their pulleys are associated, either as cause or effect, with horizontal concomitant strabismus in monkeys.

Materials and Methods

Animals and Behavioral Recordings

Ten macaque monkeys were included in the study: four with normal binocular alignment and six with strabismus. Table 1 shows the age, sex, species, ocular history, visual acuity, refractive error, and ocular motor characteristics of each animal. Each species was represented by at least one orthotropic (normal alignment) animal as a control. Esotropia developed spontaneously in the naturally strabismic monkeys before age 4 weeks[22] as documented by Ronald Boothe (Yerkes Regional Primate Center, Atlanta, GA). The artificially strabismic monkeys were reared at the Yerkes Center under conditions of contact lens occlusion or prism-goggle wear (detailed accounts of these rearing methods are contained in previous reports[23,24]).

After 4 months of age, the monkeys were shipped to Washington University in St. Louis where they were trained to fixate small tracking targets using positive-feedback rewards. Eye movements, recorded between ages 6 and 18 months using binocular magnetic search coils[25] showed the constellation of ocular motor signs that typify human infantile strabismus[26]: constant, nonparalytic heterotropia; low-velocity latent nystagmus when fixating stationary targets; and directional asymmetry of horizontal smooth pursuit or optokinetic nystagmus favoring nasally directed motion during monocular viewing. Binocular alignment was measured using automated single-cover testing as the animal fixated a stationary spot target at cardinal horizontal and vertical gaze positions.[27] As listed in Table 1, four of the strabismic animals had "pattern" strabismus, in which the horizontal angle of deviation increased or decreased in up versus down gaze. Visual acuity was measured by using the spatial-sweep visually evoked potential technique during monocular viewing.[24,28] Grating acuities were comparable in both eyes of the control and strabismic animals, with the exception of strabismic monkey RRm5, which had occlusion-induced amblyopia in the right eye. All experiments were performed in compliance with the ARVO Statement for the Use of Animals in Ophthalmic and Vision Research and were approved by the Washington University Animal Care and Use Committee.

Euthanasia and Perfusion

The animals were terminally anesthetized and perfused via the left ventricle with a solution containing 2.6% paraformaldehyde, 0.1 M lysine-HCl, 0.8% $NaIO_4$, and 0.8% iodoacetic acid (pH 7.4; modified PLP-fixative). The brain was removed for anatomic analysis, and the heads were immersed in 10% neutral-buffered formalin. Magnetic search coils were removed by minimal dissection. Including right and left orbits, 6 normal and 10 strabismic orbits were studied.

Magnetic Resonance Imaging

After warming to 38°C, formalin-fixed heads were imaged by magnetic resonance imaging (MRI) in a 1.5-T scanner (Signa; General Electric, Milwaukee, WI) with dual 10-cm phased-array surface coils. Images were T_1-weighted sequences with TR (repeat time) 400 ms and TE (echo time) 20 ms. Axial localizer scans of 3-mm thickness were first performed, as in Figure 1, with a field of view (FOV) of 8 to 10 cm and a matrix of 256 × 256 pixels for an in-plane resolution of 312 to 390 μm. Higher resolution quasicoronal images were then acquired in contiguous 1.5- to 3-mm-thick coronal planes, ranging from 15 mm posterior to 9 mm anterior to the junction of the globe and optic nerve, perpendicular to the long axis of each orbit (Fig. 2). This imaging sequence used an FOV of 4 to 6 cm over a matrix of 256 × 256 pixels, yielding an in-plane resolution of 156 to 234 μm. These images required 8 to 12 phase encodings for adequate signal-to-noise ratio. Specimen processing for the project required 5 years, during which time MRI techniques improved. This improvement is reflected in the varying resolution and slice thicknesses among the specimens. Digital MRI images were transferred to a workstation and analyzed using the program ImageJ, a public domain Java image-processing program written by Wayne Rasband (wayne@codon.nih.gov/ the Research Services Branch, National Institute of Mental Health, Bethesda, MD).

MRI Analysis

A graphic digitizing pad (Intuos A5 GD-0608U-EN; Tablet, Wacom Co., Ltd., Saitama, Japan) was used to define manually the contours of medial rectus (MR), lateral rectus (LR), and superior oblique (SO) EOMs, as well as the globe itself, in each coronal image plane. To represent EOM position, the area centroid was determined by using the "centroid" function of the ImageJ program. Next, approximating the globe as spherical, the three-dimensional (3-D) center was determined to subpixel resolution in scanner coordinates, by using a curve-fitting

function to the cross-sectional images of the globe.[29] Since the interhemispheric fissure of the brain was unavailable as a landmark, the nasal septum was chosen as the best alternative anatomic reference for normalizing the images in the yaw axis. Further, due to the absence of the ethmoid recess in the monkey, the path of the SO muscle was traced and used as an anatomic reference for pitch orientation of each orbit.

Because low contrast of EOMs with adjacent tissues is unavoidable in the postmortem MRI, it was not possible to delineate EOM cross sections in every image plane. Posteriorly, thinning of the surrounding orbital fat made it difficult to delineate structures of interest, and anteriorly, the tendons and sclera were indistinguishable. Hence, cross-sectional areas for the far anterior and posterior regions were not determined. Images of left orbits were reflected to match the spatial orientation of a right orbit for statistical analysis.

Normalization of image position and orientation was required for quantitative comparison of specimens. Magnetic field coordinates of the scanner served as reference for rotational corrections. To normalize in the quasi-coronal plane, the image was rotated to align the nasal septum with the scanner's vertical meridian. To normalize anteroposterior position, the globe-optic nerve junction was designated reference plane zero. Rectus EOM positions were translated to place the 3-D coordinate origin at the computed center of the globe. After the data were transformed, the scanner coordinates were scaled to millimeters and were then further scaled to normalize each globe to the measured average diameter of 20.93 ± 2.67 mm found by MRI. This normalization method is analogous to that used in humans[29] and was computed from the orbits of all animals in this study. This value was used to scale the EOM locations to normalize the image position and orientation. In the human literature, orbits are scaled based on globe diameter, although there are no data for any species that show that globe diameter and EOM parameters covary. At a gross level, however, such covariation seems intuitive and avoids the additional potential confound of orbital shape. In the present study, we considered the normalization necessary due to the wide age range that contributed to variation in size of structures. This shifted the centroids of EOMs differently for every animal.

To analyze the differences between cross-sectional areas of orthotropic and strabismic animals, the issue was explored statistically with a nonparametric technique appropriate to a small sample of specimens. An automated hierarchical clustering analysis was performed (JMP, ver. 3.2., statistical analysis software; SAS, Inc., Cary, NC) to test the hypothesis that strabismic animals have different horizontal EOM cross-sections than do normal animals. Cluster analysis was then repeated for each distance from the globe- optic nerve junction for which data from all specimens was represented.

Histologic Preparation

Orbits were prepared intact for histologic examination. Orbits were removed in continuity with the eyelids and orbital bones and were carefully thinned under magnification by using a high-speed drill and rongeurs. Orbits were then decalcified for 24 hours at room temperature in 0.003 M EDTA and 1.35 N HCl. Orbits were embedded in paraffin and processed for sectioning in the quasicoronal plane (perpendicular to the long axis of the orbit) at 10-μm thickness, as described previously.[8,9,30] Serial sections were mounted on 50 × 75-mm glass slides and examined microscopically after Masson's trichrome (MT) stain was applied to visualize muscle and connective tissue constituents, and van Gieson's stain to show elastin fibers.[30] The orbits of monkeys RRm5 and 1J1 were not sectioned.

Stained histologic sections were imaged in color by using a microscope equipped with objectives from 0.5× through 100× (Eclipse E800; Nikon, Tokyo, Japan) and a high-resolution digital camera (D1X; Nikon). Before quantitative analysis, micrographs were corrected for shrinkage due to histologic processing using published methods.[31] The spatially calibrated

MRI and histologic images were superimposed at partial transparency in software (Photoshop 5.5; Adobe Systems, San Jose, CA) and rotated to identical orientations. To correct for shrinkage, the histologic images were then differentially scaled in the horizontal and vertical directions so that the orbital walls were superimposed on the MRI image. Specimens were not uniformly oriented relative to the direction of the path of the knife, and so shrinkage was represented for the two arbitrary orthogonal directions required for superimposition of histologic on MRI images. All dimensional measurements were performed with micrographs individually corrected for the bidirectional shrinkage distortions stated in Table 2.

Results

Horizontal Rectus EOM Size

It was possible to obtain high-quality MRI in the cadaveric monkey specimens. Cross-sectional areas of the LR and MR EOMs were determined in each image plane in which these structures were adequately defined. Area centroids were determined by tracing as the globe equator the EOM contours (Fig. 2) from near the orbital apex to as far anteriorly as possible. Image planes were numbered relative to zero at the globe- optic nerve junction. Figure 3 illustrates MR and LR cross-section areas plotted along the lengths of the EOMs in all monkeys. In both the LR and MR of all specimens, cross-sectional area increased uniformly from the origin, peaked in midorbit, and then declined toward the insertion. Between 3 and 6 mm posterior to the globe-optic nerve junction, the cross-sectional area of the MR was at its maximum in all orbits. *M. nemestrina* specimens were older than those of the other species, and these specimens exhibited larger horizontal rectus EOM cross sections than did the other species. For each EOM, the cross sectional area was maximal in midorbit, but there was considerable variability in cross-sectional area among animals. With the small population of monkeys available, we segregated the data based on ocular alignment, and found variability between the monkeys, primarily due to the wide age range. Despite the differences among these animals, the trend for the EOM cross-sectional area remained the same. We did not attempt to describe the variability that may be introduced by gender or species. Exceptionally large cross-sections (Fig. 3, 79434) were obtained from a 22-year-old naturally esotropic *M. nemestrina*, the oldest and largest of all specimens. Data from monkey 79434 was therefore excluded from the computed mean values, because this animal was an outlier. Monkeys 1J1 (right orbit), 79434 (left orbit), and 124G (left orbit) did not have sufficiently clear images of EOMs to make reliable cross-sectional measurements. Table 2 shows the mean maximum cross-sectional areas of the MR and LR EOMs in normal and strabismic monkeys measured from histology after correcting for shrinkage.

Although Figure 3 suggests no obvious differences between orthotropic and strabismic animals, the difference was explored statistically with an automated hierarchical clustering analysis. If horizontal rectus EOMs in strabismic monkeys differs from those of orthotropic monkeys, the cross-sectional area data from these two groups should cluster significantly differently from one another. Instead, the dendrograms for all image planes (−7 through +6) clustered primarily according to cross-sectional area of EOM, and the remainder of the clustering was not based on any specific category such as species, age, or gender, with no clustering according to binocular alignment or laterality (Fig. 4). The outlier monkey (79434) was included in the analysis, but segregated uniquely, as expected.

Figure 5 shows coronal MRIs of both orbits in a normal and in a *Macaca mulatta* with induced exotropia, demonstrating the ALR in each. The ALR was either not observable or was too small for reliable study by MRI in most of the monkeys, and so was histologically evaluated instead. It was bilaterally evident in all orbits examined histologically. Table 2 shows the mean maximum ALR, MR, and LR cross-sectional areas of each orbit. Data from three normal monkeys were compared with those of five strabismic animals, for a total of 11 orbits. The

cross section of the ALR, however, was less than 9% of LR cross section in orthotropic and less than 15% of LR cross section in strabismic monkeys, and its cross section also varied widely among animals. Mean ALR cross-sectional area in normal monkeys was 1.2 ± 0.5 mm^2, not significantly different from the value of 2.0 ± 1.0 mm^2 ($P = 0.16$) in esotropic monkeys and 1.2 ± 0.1 mm^2 in the exotropic monkey. Mean ALR length was 15.1 ± 3.3 mm, in contrast to the mean lengths of 33.0 ± 4.6 and 38.5 ± 4.1 mm for the MR and LR, respectively.

Horizontal Rectus EOM Paths

Figure 6 plots the normalized horizontal coordinates of horizontal rectus EOM paths as functions of anteroposterior location distance from the junction of the globe and optic nerve, demonstrating EOM paths in superior view. The MRI followed a nearly straight anteroposterior path, but the LR path was inclined temporally due to temporal angulation of the orbit relative to the midsagittal plane. There was no significant EOM path difference between the left and right orbits. The LR path was more angled in the monkeys with shallower orbits. In monkey 124G, only the right orbit was imaged before histologic sectioning.

Figure 7 plots in lateral view the normalized vertical coordinates of horizontal rectus EOM centroids as functions of anteroposterior location distance from the junction of the globe and optic nerve, demonstrating EOM paths in lateral view. The horizontal rectus EOMs from the left orbit were consistently slightly higher than those of the right orbit, suggesting imperfect bilateral symmetry.

In cadaveric specimens there are no EOM path inflections to indicate pulley locations. Therefore, it was assumed that the coronal plane locations of the rectus pulleys corresponded to the most anterior coordinates of the EOM centroids obtainable in MRI images, which were 2 to 6 mm anterior to the globe-optic nerve junction. Rectus EOM paths were similar between normal and strabismic monkeys (Figs. 6, 7). Hierarchical cluster analysis showed no tendency toward distinct segregation of pulley locations between normal and strabismic animals. Dendrograms of MR and LR pulley locations, taken to be at the most anterior plane in which EOM centroids could be resolved, showed no clustering based on species, age, gender, binocular alignment, or laterality.

Histologic sectioning was not continued to a depth sufficient to study the complete length of the rectus EOMs. Instead, axial MRI was used to measure the anteroposterior length of the horizontal rectus EOMs. The mean length of the normal LR muscle was 38.3 ± 4.0 mm. Mean LR length was 35.7 ± 1.3 mm in esotropic ($P = 0.14$) and 44.6 ± 1.1 mm in exotropic ($P = 0.80$) monkeys. Mean normal MR length was 32.3 ± 2.4 mm. Mean MR length was 29.6 ± 1.7 mm ($P = 0.06$) in esotropic and 40.8 ± 1.3 mm ($P = 0.19$) in exotropic animals.

Mean ALR length averaged 15.8 ± 4.5 mm in normal, 15.5 ± 2.6 mm in esotropic ($P = 0.9$), and 10.6 mm in exotropic monkeys. The length of the ALR relative to overall orbit length was 0.8 in normal, 0.7 in esotropic, and 0.5 in exotropic monkeys. Older, and consequently larger, monkeys had ALRs that were longer than the younger animals. Subject RYu6 had prism-induced infantile exotropia but the shortest ALR at 10.6 mm. Figure 8 shows ALR location in the coronal plane at the junction of the globe and optic nerve, as well as locations of the LR, SR, and optic nerve (ON). The coordinate system origin is at globe center. Although variable, the graph shows that the ALR location did not differ significantly between normal and strabismic monkeys.

Histology of Horizontal Rectus EOMs and Pulleys

Histologic sections were used to examine features not well demonstrated by MRI. The sections were of high quality due to interarterial perfusion of fixative. Figure 9 shows coronal histologic

sections, stained with MT, of the right orbit of naturally esotropic nemestrina monkey 124G. EOM fibers in the stained sections were indicated in red and collagen in blue. Muscle and connective tissue features were demonstrated in detail throughout the orbit. Figure 10 allows comparison of micrographs of the LR and MR pulleys in a normal, a naturally esotropic, and an artificially esotropic monkey. Sections stained with van Gieson's elastin stain (EVG) indicated elastin fibrils in black (Fig. 10). In both normal and strabismic monkeys, the MR and LR EOMs exhibited distinct global (GL) and orbital (OL) layers. Fibers in the OL were located in a C-shaped layer near the orbital surface and had smaller-diameter and darker-staining fibers. Fibers in the GL formed the core of EOMs and had larger and brighter red staining fibers. Horizontal rectus EOMs were similar among all specimens, with no distinguishing characteristics in strabismic animals. Anterior regions of the horizontal rectus EOMs were surrounded by fibroelastic sleeves consisting predominantly of collagen. The densest parts of the sleeves were reinforced by elastic fibers (Fig. 10) and constituted the pulley rings, as described elsewhere.[9] There were no differences in pulley features between normal and strabismic monkeys.

Histology of Horizontal Rectus EOM Innervation

The MR muscle is innervated by a branch of the inferior division of the oculomotor nerve, whereas the LR is innervated by the abducens nerve. These motor nerves were demonstrable in the deep orbits of all specimens and bifurcated repeatedly on the orbital surface of each EOM as they coursed anteriorly to enter the EOM in multiple sites. All specimens exhibited motor nerves of comparable size in the horizontal rectus EOMs and comparable intramuscular motor nerve arborizations within these EOMs.

Intramuscular nerve density was calculated by counting every axon in all the transversely sectioned nerve bundles, in each of six histologic sections of the horizontal rectus EOMs in the region in which visual inspection indicated maximum nerve arborization. Axons within nerve bundles that were oblique to the plane of section were not counted. The number of axons in each section was divided by that section's cross-sectional area to obtain the nerve density (the number of axons per square millimeter of EOM), which was averaged over the six histologic sections analyzed for the EOM. Table 2 shows the nerve density in the ALR, LR, and MR.

Monkey RKb3 had a tearing artifact in the histologic sections and REd3 was a 6-month-old monkey with insufficient EOM length to average over several planes for nerve density. Hence, these two animals were not analyzed for nerve density. Although the data are variable among monkeys, they do not indicate any systematic association between strabismus and motor nerve density in the horizontal rectus EOMs.

In all specimens, the ALR originated on the orbital surface of the deep LR belly, and inserted on the posterior globe between the LR and SR EOMs. The ALR was small and inconsistently located, but always had a posterior insertion on the sclera, providing little mechanical advantage for ocular rotation. The ALR had only a single layer, resembling the GL of the oculorotary EOMs, and exhibited very sparse innervation in comparison with the oculorotary EOMs (Fig. 11). The ALR was never surrounded by any significant connective tissue sleeve suggestive of a pulley.

Discussion

Strabismus occurs in both humans[17] and monkeys,[32] and features of their rectus EOMs and pulleys are correspondingly similar.[9] The simian model has thus been used to understand the etiology, consequences, and treatments of human strabismus.[23,24,33–37] In the current study, we investigated orbital anatomy in monkeys with natural or artificial strabismus, comparing

findings with those in orthotropic animals. Because cadaveric MRI does not distinguish tendons and connective tissue in the most anterior orbit, histologic examination of whole orbits was also performed. The configuration, paths, cross-sectional areas, pulleys, and innervation of the MR and LR were similar to normal in both naturally and artificially strabismic monkeys. The ALR, which was universally present, was nevertheless small and exhibited no relationship to strabismus. Even the “A” and “V” patterns observed in the strabismic monkeys were not reflected in rectus pulley positions, indicating that whereas rectus pulley heterotopy may be sufficient for such incomitance,[12,13] heterotopy is not necessary. This finding is consistent with single-unit motoneuron recordings, suggesting that incomitance in monkeys with induced strabismus has a central innervational basis.[38]

The sample size examined was necessarily small. However, the absence of abnormalities associated with strabismus makes it unlikely that a mechanical or cranial nerve disease is causative of infantile or developmental strabismus in the animals examined, and instead supports the proposition that this type of strabismus is caused by supranuclear innervational factors.[39] Several cerebral factors in infant primates may contribute to strabismus. These factors include weak horizontal connections and high indices of suppression between ocular dominance columns in the visual cortex, as well as innate biases favoring both convergence and nasally directed motion in immature eye movement pathways.[40–43] The present study showed that infantile strabismus, occurring naturally or induced artificially in primates, is associated with neither abnormalities of horizontal rectus EOM size, nor the connective tissue pulleys that influence the EOM paths. Whereas both EOM hypoplasia[44] and pulley heterotopy[12,13,45–48] apparently cause some cases of strabismus, such abnormalities were absent and could not have caused the natural strabismus in the monkeys that we studied. Conversely, artificial strabismus in the present group of monkeys did not cause abnormalities of horizontal rectus EOMs or their pulleys. Developmental strabismus in this sample of monkeys was unrelated to detectable peripheral neural abnormalities. It remains possible that the EOMs and orbits of strabismic moneys harbored abnormalities not detectable by the methods that we used, but the present study can reasonably exclude gross and light microscopically detectable disease. To the degree that these monkeys model human infantile and developmental strabismus, these conclusions may be applicable to humans.

Monkeys have an ALR innervated by an abducens nerve branch.[49] Although some investigators have proposed that the ALR represents an atavistic retractor bulbi (RB) residual from lower vertebrates,[49] the ALR is dissimilar to the RB, in that the ALR originates on the LR. In lower vertebrates, the RB has four broad heads originating in the optic foramen.[19] These differences motivated the suggestion that the ALR is an elevator and abductor[21] with an oculorotatory tonus that could constitute one factor that increases the resistance of monkeys to the development of esotropia. Conversely, the human propensity to infantile esotropia was proposed to arise in part from the absence of the ALR.[21]

The present study demonstrated important differences between the ALR and oculorotatory EOMs. Similar to the levator palpebrae superioris but unlike the rectus and oblique EOMs, the ALR lacks both an orbital layer and a pulley. Although its unit moment vector in primary position reportedly gives the ALR an abducting and elevating action,[21] the posterior insertion and absence of a pulley gives the ALR almost no tangency with the globe during ductions. The ALR pulls nearly perpendicular to the globe in central gaze (Table 2› Fig. 8). Consequently, the ALR's pulling direction must change markedly, and even reverse, during large ductions. Such variable mechanical behavior is atypical of the rectus and oblique EOMs, whose paths are constrained in an orderly fashion by pulleys.[7] These considerations support the proposition that the ALR is vestigal[49] and has so little oculorotatory action that it is unlikely to contribute to strabismus in any way. The length and location of the ALR did not differ significantly between orthotropic and strabismic monkeys. The present study confirms that the ALR is

considerably smaller than the rectus EOMs.[21,49] The monkey ALR generates only one seventh the tension of the LR, and does so much more slowly.[50] Because the ALR is approximately one tenth the cross-sectional area and half the length of a rectus EOM, it is difficult to envision that it plays a significant mechanical role in ocular motility.

Unlike the rectus and oblique EOMs, the ALR reportedly contains only singly innervated fibers and lacks multiply innervated fibers.[49] The present study reports the novel finding of markedly sparse ALR innervation, with a density only approximately 20% that of rectus EOMs. Sparse innervation is consistent with slow development of ALR tension during electrical stimulation.[50] The absence of the ALR in humans probably has no significant effect in promoting strabismus.

Acknowledgements

The authors thank Nicolasa De Salles and Frank Henriquez for technical assistance.

Supported by U.S. Public Health Service National Eye Institute Grant EY-08313 and Core Grant EY-00331. JLD received a Research to Prevent Blindness Walt and Lilly Disney Award for Amblyopia Research, and is the Leonard Apt Professor of Ophthalmology.

References

1. Miller, JM. Computer model of binocular alignment. In: Semmlow, JL.; Welkowitz, W., editors. Sixth Annual Conference, IEEE Engineering in Medicine and Biology Society. New York: IEEE; 1984.
2. Miller, JM.; Pavlovski, DS.; Shaemeva, I. Orbit 1.8 Gaze Mechanics Simulation. San Francisco: Eidactics; 1999.
3. Robinson DA. A quantitative analysis of extraocular muscle cooperation and squint. Invest Ophthalmol Vis Sci 1975;14:801–825.
4. Miller JM, Robins D. Extraocular muscle sideslip and orbital geometry in monkeys. Vision Res 1987;27:381–392. [PubMed: 3660599]
5. Simonsz HJ, Harting F, de Waal BJ, Verbeeten BWJM. Sideways displacement and curved path of recti eye muscles. Arch Ophthalmol 1985;103:124–128. [PubMed: 3977665]
6. Miller JM. Functional anatomy of normal human rectus muscles. Vision Res 1989;29:223–240. [PubMed: 2800349]
7. Demer JL. Pivotal role of orbital connective tissues in binocular alignment and strabismus: The Friedenwald Lecture. Invest Ophthalmol Vis Sci 2004;45:729–738. [PubMed: 14985282]
8. Demer JL, Oh SY, Clark RA, Poukens V. Evidence for a pulley of the inferior oblique muscle. Invest Ophthalmol Vis Sci 2003;44:3856–3865. [PubMed: 12939301]
9. Demer JL, Poukens V, Miller JM, Micevych P. Innervation of extraocular pulley smooth muscle in monkeys and humans. Invest Ophthalmol Vis Sci 1997;38:1774–1785. [PubMed: 9286266]
10. Oh SY, Poukens V, Demer JL. Quantitative analysis of rectus extraocular muscle layers in monkey and humans. Invest Ophthalmol Vis Sci 2001;42:10–16. [PubMed: 11133842]
11. Clark RA, Miller JM, Demer JL. Three-dimensional location of human rectus pulleys by path inflections in secondary gaze positions. Invest Ophthalmol Vis Sci 2000;41:3787–3797. [PubMed: 11053278]
12. Clark RA, Miller JM, Rosenbaum AL, Demer JL. Heterotopic muscle pulleys or oblique muscle dysfunction? J AAPOS 1998;2:17–25. [PubMed: 10532362]
13. Demer, JL.; Clark, RA.; Miller, JM. Heterotopy of extraocular muscle pulleys causes incomitant strabismus. In: Lennerstrand, G., editor. Advances in Strabismology. Buren, The Netherlands: Aeolus Press; 1999. p. 91-94.
14. Krzizok T, Wagner D, Kaufmann H. Elucidation of restrictive motility in high myopia by magnetic resonance imaging. Arch Ophthalmol 1996;115:1019–1027.
15. Krzizok TH, Kaufman H, Traupe H. New approach in strabismus surgery in high myopia. Br J Ophthalmol 1997;81:625–630. [PubMed: 9349146]

16. Krzizok TH, Schroeder BU. Measurement of recti eye muscle paths by magnetic resonance imaging in highly myopic and normal subjects. Invest Ophthalmol Vis Sci 1999;40:2554–2560. [PubMed: 10509649]

17. von Noorden, GK. Binocular Vision and Ocular Motility: Theory and Management of Strabismus. 4. St. Louis: Mosby; 1990.

18. Boothe RG, Kiorpes L, Carlson MR. Studies of strabismus and amblyopia in infant monkeys. J Pediatr Ophthalmol Strabismus 1985;22:206–212. [PubMed: 4045651]

19. Haines DE, Holmes KR, Bollert JA. Eye muscles in monkey and man. Mich Acad 1969;30:13–20.

20. Harwerth R, Smith E. Rhesus monkey as a model for normal vision of humans. Am J Optom Physiol Opt 1985;62:633–641. [PubMed: 4050966]

21. Boothe RG, Quick M, Josse MV, Abbas MA, Anderson DC. ALR orbital geometry in normal and naturally strabismic monkeys. Invest Ophthalmol Vis Sci 1990;31:1168–1174. [PubMed: 2354917]

22. Kiorpes L, Boothe RG. Naturally occurring strabismus in monkeys (*Macaca nemestrina*). Invest Ophthalmol Vis Sci 1981;20:257–263. [PubMed: 7461928]

23. Tychsen L, Scott C. Maldevelopment of convergence eye movements in macaque monkeys with small- and large-angle infantile esotropia. Invest Ophthalmol Vis Sci 2003;44:3358–3368. [PubMed: 12882782]

24. Wong AM, Foeller P, Bradley D, Burkhalter A, Tychsen L. Early versus delayed repair of infantile strabismus in macaque monkeys: I. ocular motor effects. J AAPOS 2003;7:200–209. [PubMed: 12825061]

25. Foeller P, Tychsen L. Eye movement training and recording in alert macaque monkeys: 1. Operant visual conditioning 2. Magnetic search coil and head restraint surgical implantation 3. Calibration and recording. Strabismus 2002;10:5–22. [PubMed: 12185647]

26. Tychsen, L.; Yildirim, C. Macaque monkey as an ocular motor and neuroanatomic model of human infantile strabismus. In: Lennerstrand, G.; Ygge, J., editors. Advances in Strabismus Research: Basic and Clinical Aspects. London: Portland Press; 2000. p. 103-119.

27. Scott C, Gusdorf G, Tychsen L. Automated cover test for eye misalignment in awake monkeys using spectacle-mounted liquid crystal shutters. Binocul Vis Strabismus Q 2000;15:59–66. [PubMed: 10767684]

28. Norcia AM, Tyler CW. Spatial frequency sweep VEP: visual acuity during the first year of life. Vision Res 1985;25:1399–1408. [PubMed: 4090273]

29. Clark RA, Miller JM, Demer JL. Location and stability of rectus muscle pulleys: muscle paths as a function of gaze. Invest Ophthalmol Vis Sci 1997;38:227–240. [PubMed: 9008649]

30. Demer JL, Miller JM, Poukens V, Vinters HV, Glasgow BJ. Evidence for fibromuscular pulleys of the recti extraocular muscles. Invest Ophthalmol Vis Sci 1995;36:1125–1136. [PubMed: 7730022]

31. Kono R, Poukens V, Demer JL. Quantitative analysis of the structure of the human extraocular muscle pulley system. Invest Ophthalmol Vis Sci 2002;43:2923–2932. [PubMed: 12202511]

32. Tychsen L, Wong AM, Burkhalter A. Paucity of horizontal connections for binocular vision in V1 of naturally strabismic macaques: cytochrome oxidase compartment specificity. J Comp Neurol 2004;474:261–275. [PubMed: 15164426]

33. Tychsen L, Burkhalter A. Nasotemporal asymmetries in V1: ocular dominance columns of infant, adult, and strabismic macaque monkeys. J Comp Neurol 1997;388:32–46. [PubMed: 9364237]

34. Tychsen L, Wong AM, Foeller P, Bradley D. Early versus delayed repair of infantile strabismus in macaque monkeys: II. Effects on motion visually evoked responses. Invest Ophthalmol Vis Sci 2004;45:821–827. [PubMed: 14985296]

35. Wong AM, Burkhalter A, Tychsen L. Suppression of metabolic activity caused by infantile strabismus and strabismic amblyopia in striate visual cortex of macaque monkeys. J AAPOS 2005;9:37–47. [PubMed: 15729279]

36. Yildirim C, Tychsen L. Effect of infantile strabismus on visuomotor development in the squirrel monkey (*Saimiri sciureus*): optokinetic nystagmus, motion VEP and spatial sweep VEP. Strabismus 1999;7:211–219. [PubMed: 10694912]

37. Yildirim C, Tychsen L. Disjunctive optokinetic nystagmus in a naturally esotropic macaque monkey: interaction between nasotemporal asymmetries of versional eye movement and convergence. Ophthalmic Res 2000;32:172–180. [PubMed: 10828738]

38. Das VE, Mustari MJ. Correlation of cross-axis eye movements and motoneuron activity in non-human primates with “A” pattern strabismus. Invest Ophthalmol Vis Sci 2007;48:665–674. [PubMed: 17251464]
39. von Noorden, GK.; Tychsen, L. Infantile esotropia: Current neurophysiologic concepts. In: Rosenbaum, AL.; Santiago, AP., editors. Clinical Strabismus Management. Philadelphia: WB Saunders; 1999. p. 117-138.
40. Chino YM, Smith ELI, Hatta S, Cheng H. Postnatal development of binocular disparity sensitivity in neurons of primate visual cortex. J Neurosci 1997;17:296–307. [PubMed: 8987756]
41. Endo M, Kaas JH, Neeragi J, Smith ELI, Chino YM. Binocular cross-orientation suppression in primary visual cortex (V1) of infant rhesus monkeys. Invest Ophthalmol Vis Sci 2000;41:4022–4031. [PubMed: 11053308]
42. Horwood AM, Riddell PM. Can misalignments in typical infants be used as a model for infantile esotropia? Invest Ophthalmol Vis Sci 2004;45:714–720. [PubMed: 14744919]
43. Tychsen, L. Strabismus: The Scientific Basis. In: Taylor, D.; Hoyt, C., editors. Pediatric Ophthalmology and Strabismus. Edinburgh: Elsevier Saunders; 2005. p. 836-848.
44. Demer JL, Clark RA, Engle EC. Magnetic resonance imaging evidence for widespread orbital dysinnervation in congenital fibrosis of extraocular muscles due to mutations in KIF21A. Invest Ophthalmol Vis Sci 2005;46:530–539. [PubMed: 15671279]
45. Clark RA, Miller JM, Demer JL. Displacement of the medial rectus pulley in superior oblique palsy. Invest Ophthalmol Vis Sci 1998;39:207–212. [PubMed: 9430565]
46. Demer, JL.; Velez, FG.; Clark, RA.; Oh, SY. Abstracts of 26th Annual Meeting of the American Association for Pediatric Ophthalmology and Strabismus. San Francisco, CA: AAPOS; 2000. Rectus extraocular muscle (EOM) pulley instability: a cause of incomitant strabismus (abstract); p. 6pSan Diego, CA. April 2000
47. Oh SY, Clark RA, Velez F, Rosenbaum AL, Demer JL. Incomitant strabismus associated with instability of rectus pulleys. Invest Ophthalmol Vis Sci 2002;43:2169–2178. [PubMed: 12091413]
48. Velez FG, Clark RA, Demer JL. Facial asymmetry in superior oblique palsy and pulley heterotopy. J AAPOS 2000;4:233–239. [PubMed: 10951300]
49. Schnyder H. The innervation of the monkey ALR muscle. Brain Res 1984;296:139–144. [PubMed: 6201232]
50. Fuchs AF, Luschei ES. Development of isometric tension in simian extraocular muscle. J Physiol (Lond) 1971;219:155–166. [PubMed: 5003481]

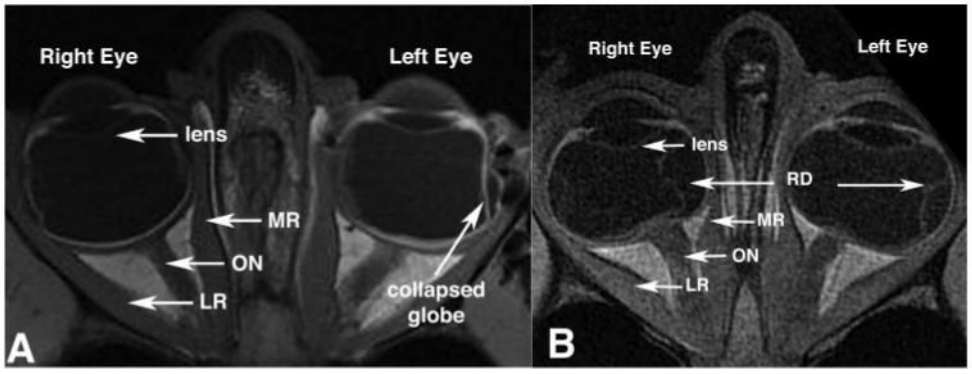

Figure 1.

Axial MRIs showed no systematic differences between the orbits of orthotropic and strabismic monkeys. *Left*: orthotropic *M. mulatta* 94D248. Resolution, 273 μm in a 3-mm-thick plane. *Right*: artificially induced right esotropic *M. mulatta* RRm5, which had undergone monocular occlusion of the right eye. Resolution, 234 μm in 2-mm-thick plane. RD, retinal detachment.

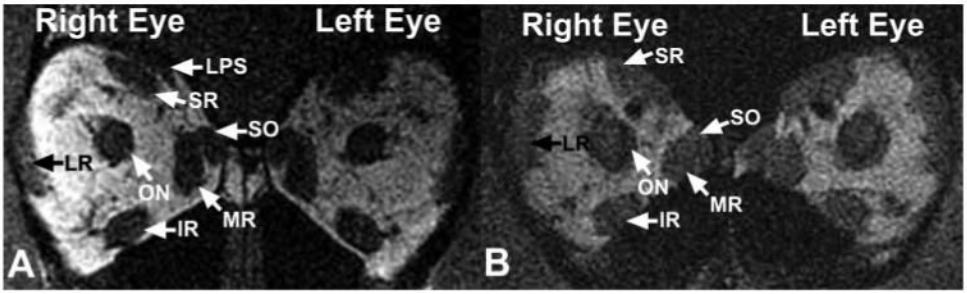

Figure 2.

Quasicoronal MRIs taken 9 mm posterior to the globe- optic nerve junction demonstrated no systematic differences between orbits of normal and strabismic monkeys. *Left*: orthotropic *Macaca nemestrina* 80478. Resolution, 312 μm in 2-mm-thick image planes. *Right*: naturally esotropic *M. nemestrina* 124G. Resolution, 390 μm in 3-mm-thick image planes. IR, inferior rectus muscle; LPS, levator palpebrae superioris muscle.

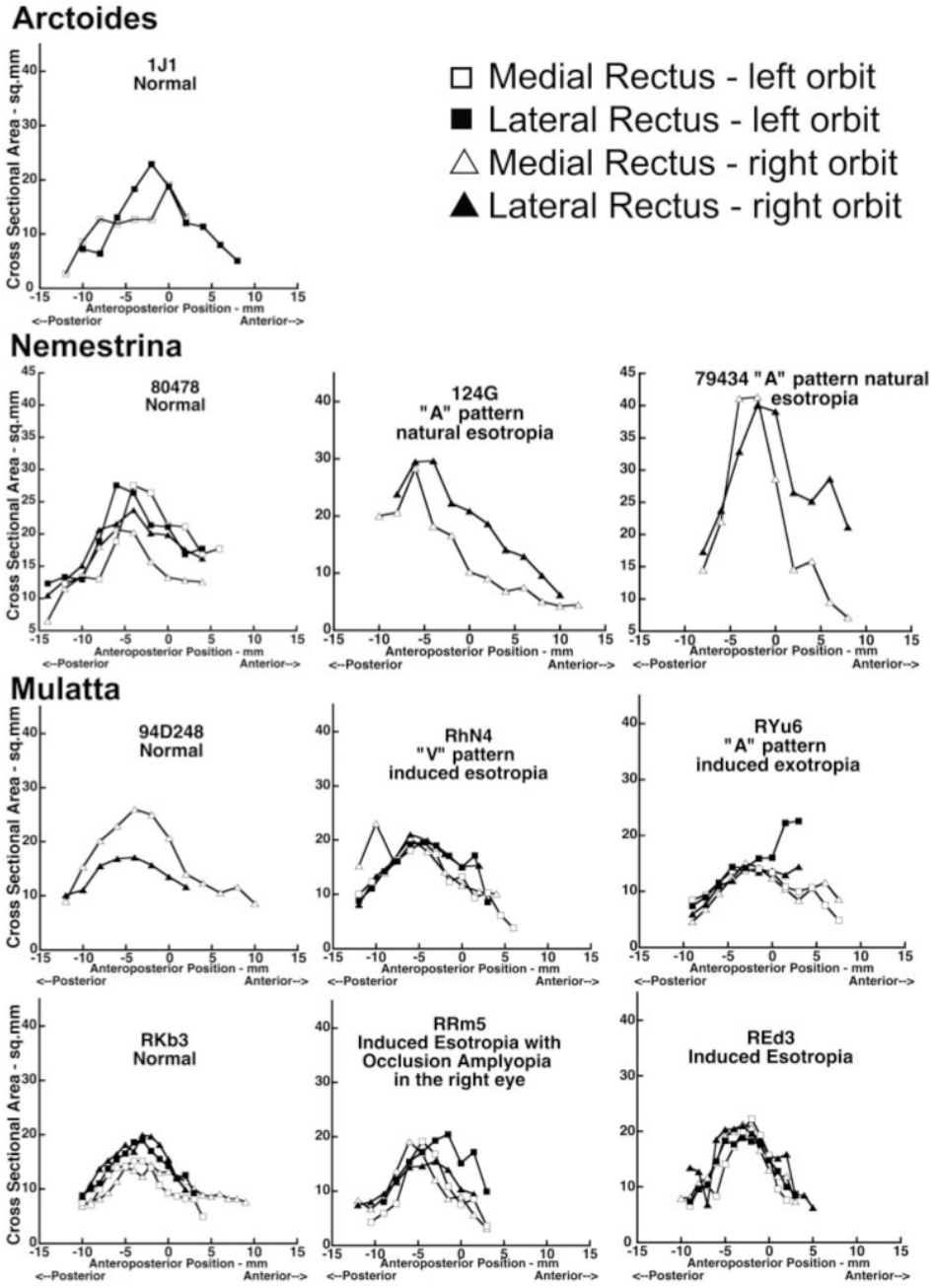

Figure 3.

Cross-sectional areas of the MR and LR in normal and strabismic monkeys plotted against anteroposterior distance along the muscles, relative to 0 at the globe- optic nerve junction.

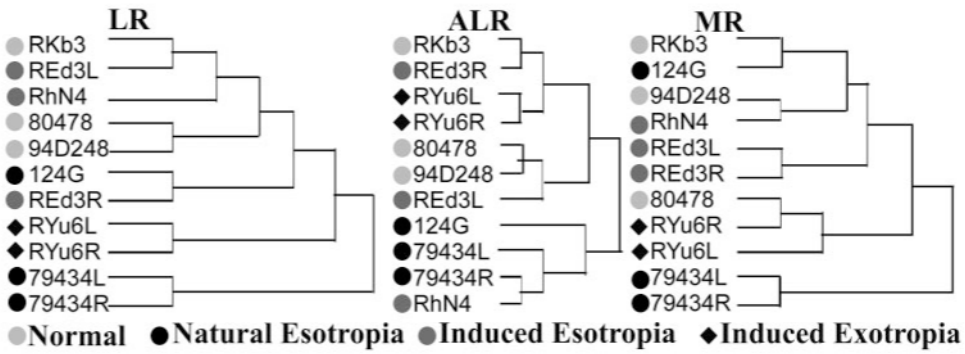

Figure 4.

Hierarchical clustering analysis based on cross-sectional areas of the MR, LR, and ALR in normal and strabismic monkeys. Clustering did not occur according to binocular alignment or laterality, species, age, or gender.

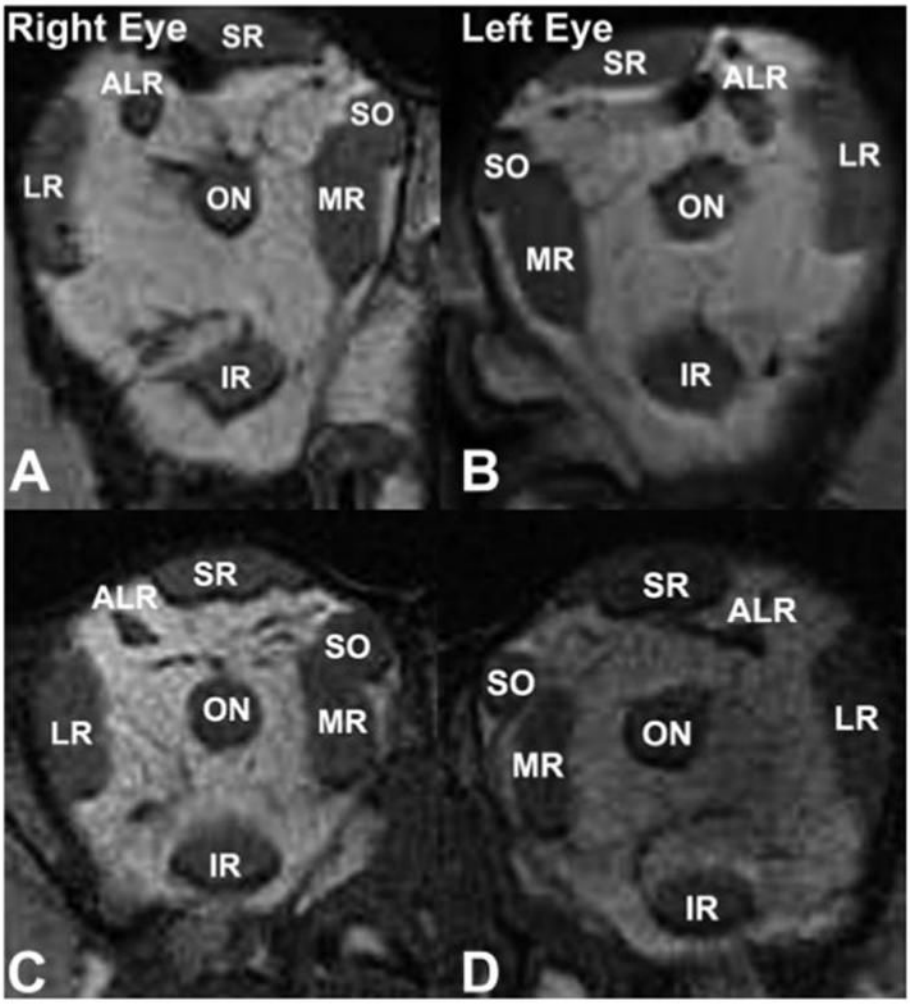

Figure 5.
Quasicoronal MRI of the right and left orbits of monkeys 1.5 to 2 mm posterior to the globe-optic nerve junction. (**A**, **B**) Orthotropic *M. mulatta* 94D248. Resolution, 234 μm in 2-mm-thick image planes. (**C**, **D**) Induced exotropic *M. mulatta* RYu6. Resolution, 234 μm in 1.5-mm-thick image planes. IR, inferior rectus muscle.

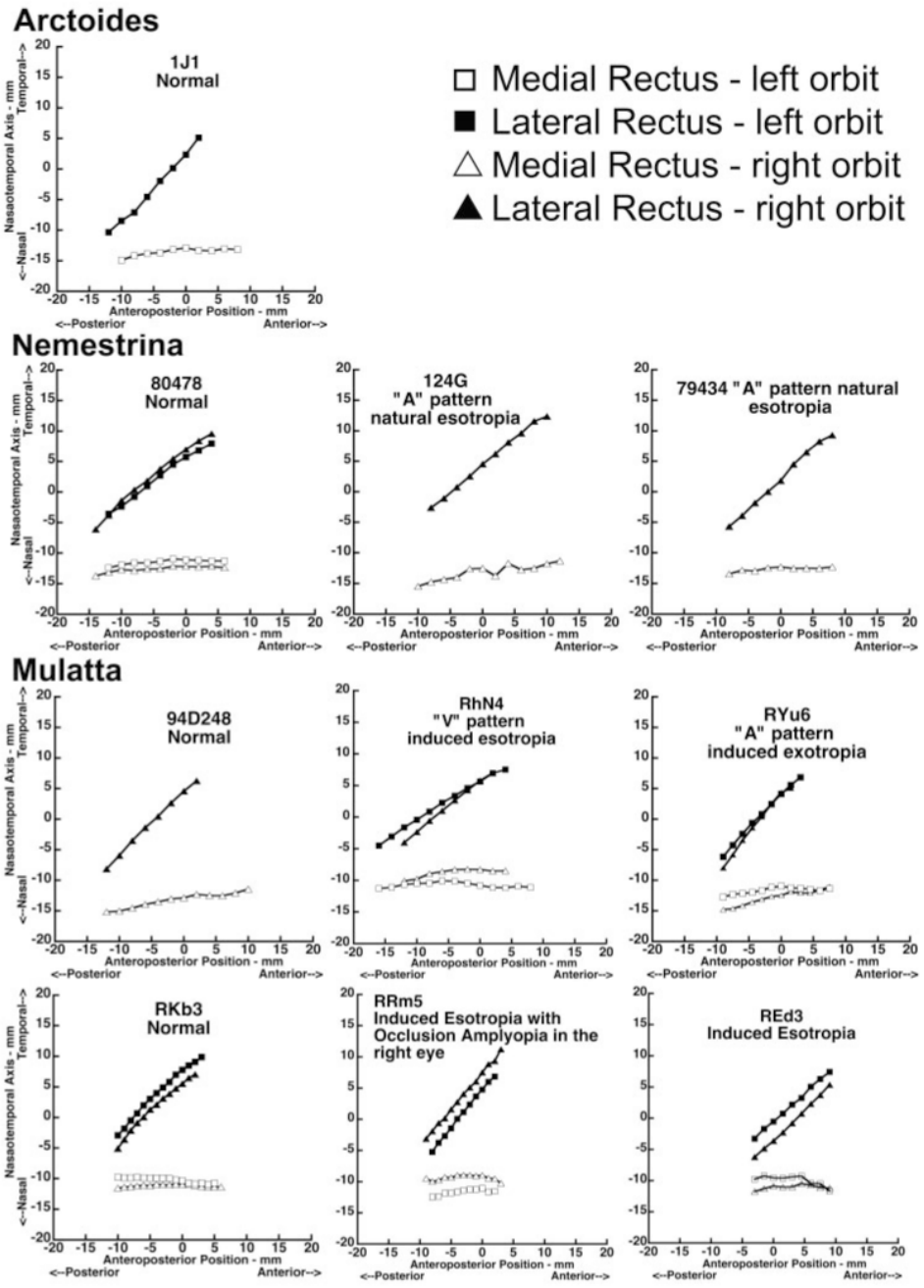

Figure 6.
Horizontal coordinates of horizontal rectus EOM paths along the orbit for both normal and strabismic monkeys, 0 at the globe- optic nerve junction.

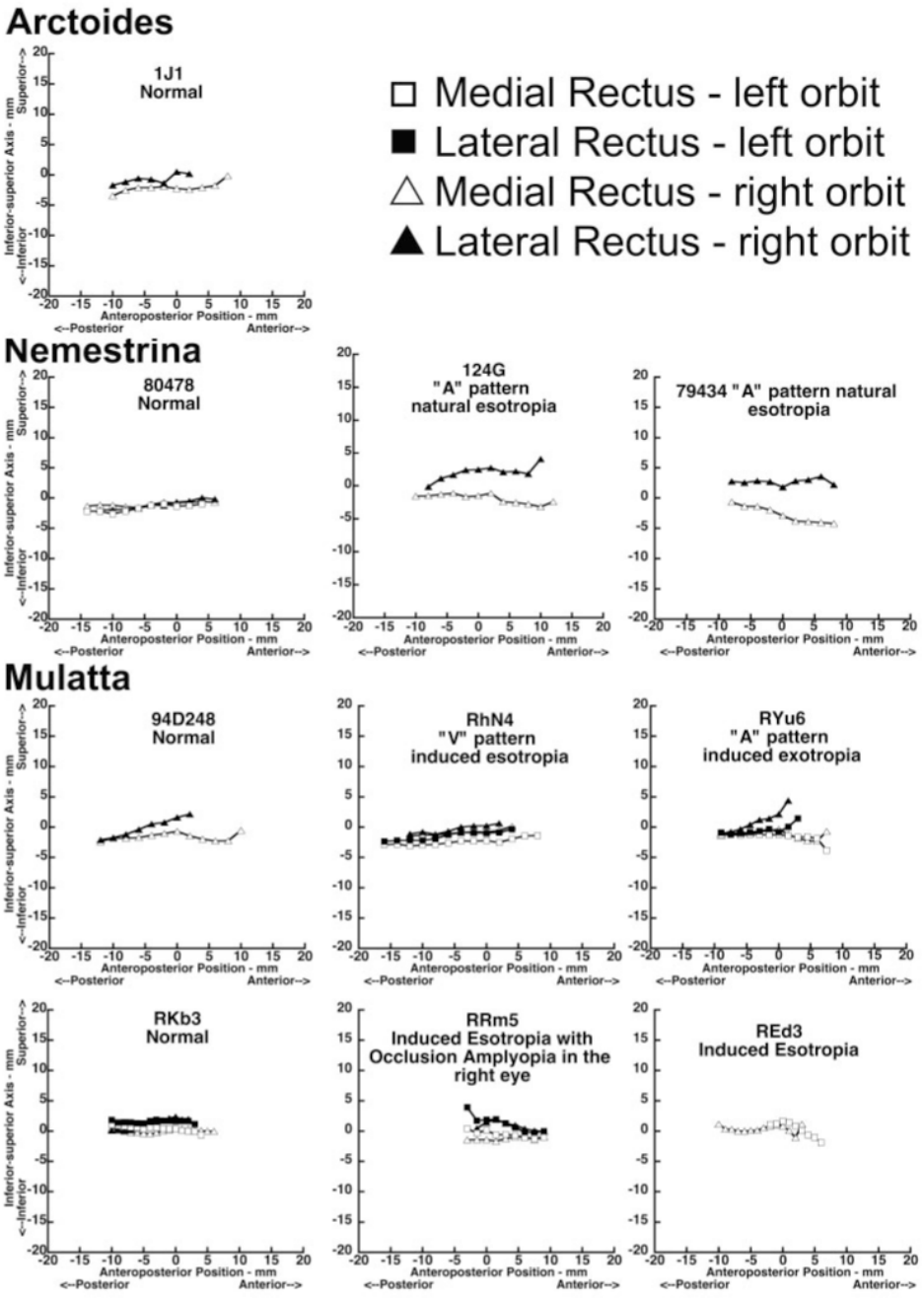

Figure 7.

Vertical coordinates of horizontal rectus EOM paths for the normal and strabismic monkeys. Anteroposterior positions are relative to 0, at the globe- optic nerve junction.

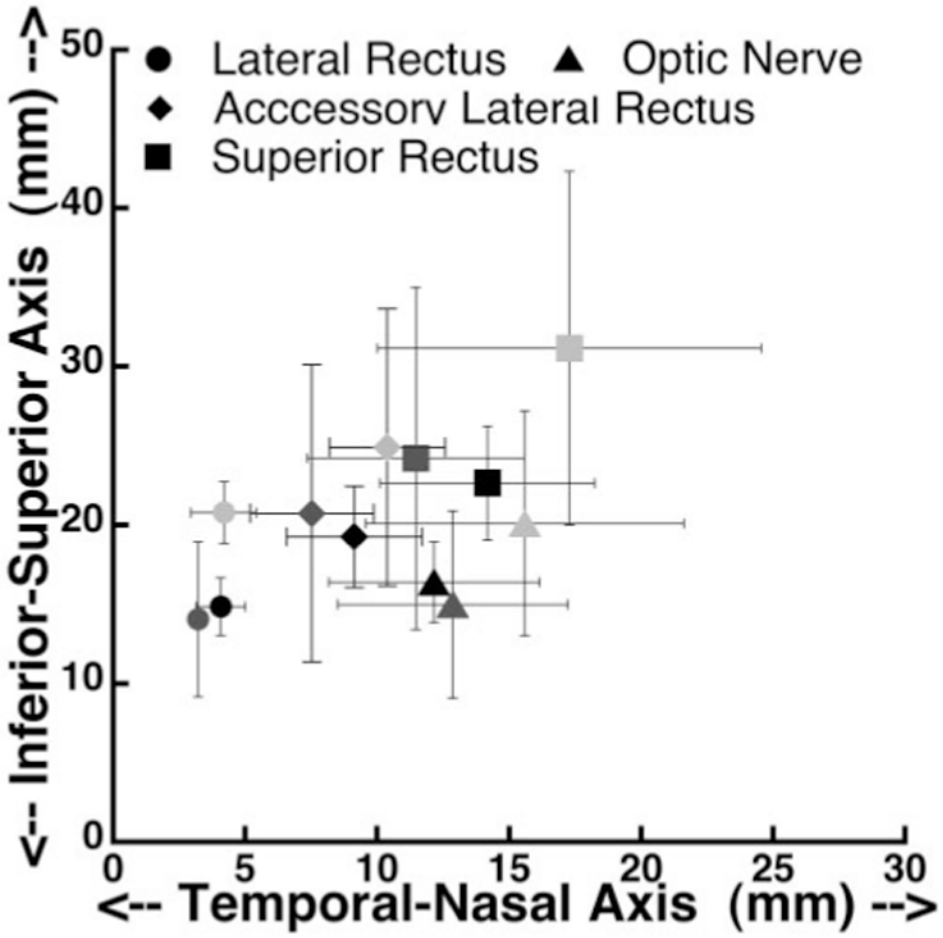

Figure 8.
Location of accessory lateral rectus muscle at the anteroposterior level of the globe and optic nerve junction, in comparison to the optic ON and the LR and SR muscles. *Light gray symbols*: normal monkeys; *black symbols*: esotropic monkeys; *dark gray symbols*: exotropic monkey.

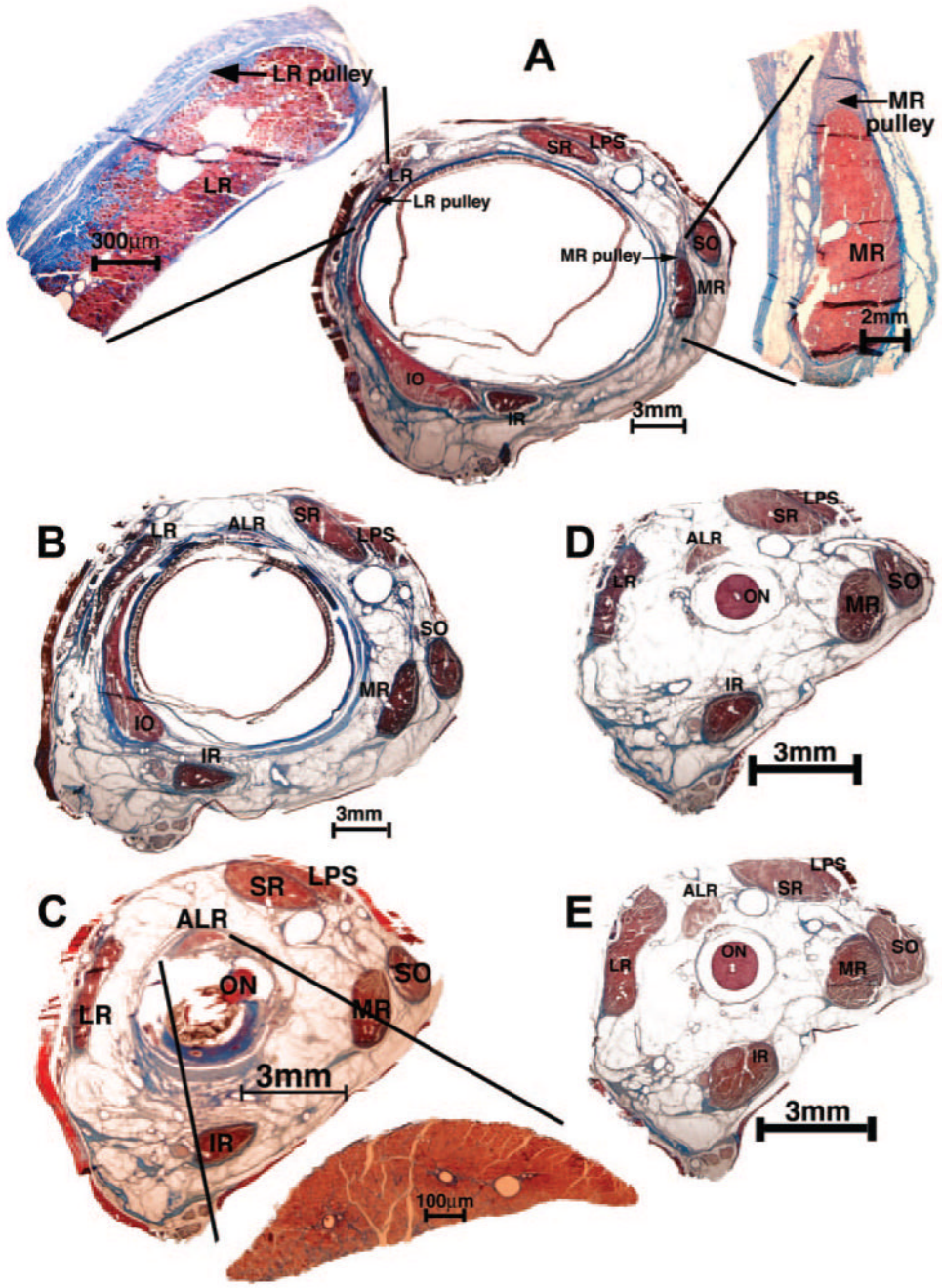

Figure 9.

Histologic sections in the quasicoronal plane from right orbit of naturally esotropic monkey 124G stained with MT. (**A**) In the pulley region 4 mm anterior to globe- optic nerve junction. The LR and MR muscles are magnified in adjacent insets. (**B**) Two millimeters anterior to the globe- optic nerve junction. This region is immediately posterior to the rectus pulleys. (**C**) At the globe- optic nerve junction, well posterior to the pulleys. *Inset*: magnified view of the ALR. (**D**) Two millimeters and (**E**) 4 mm posterior to the globe- optic nerve junction. LPS, levator palpebrae superioris muscle; IR, inferior rectus muscle.

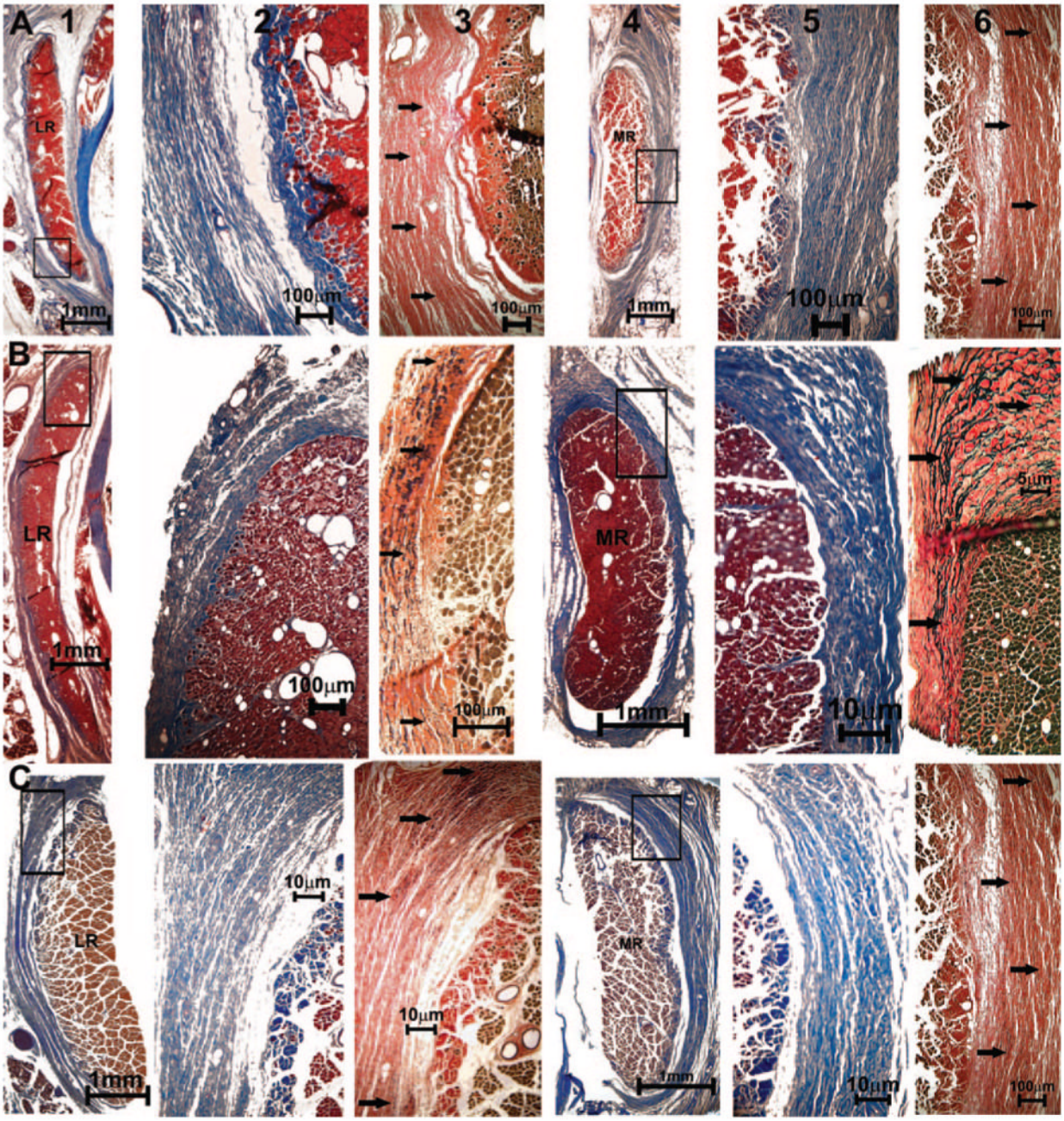

Figure 10.

Quasicoronal histologic sections of monkey orbits stained with MT and EVG stains. (**A**) Normal (94D248 right orbit), (**B**) naturally esotropic (124G left orbit), and (**C**) artificially esotropic (RHn4 left orbit) monkeys. *Columns* from *left* to *right*: lateral rectus (LR) EOM (1), magnified inset of pulley in MT stain (2), and elastin fibrils (*arrows*) in EVG stain (3), MR EOM (4), magnified *inset* of collagen fibers in MT stain (5), and elastin fibrils (*arrows*) in EVG stain (6).

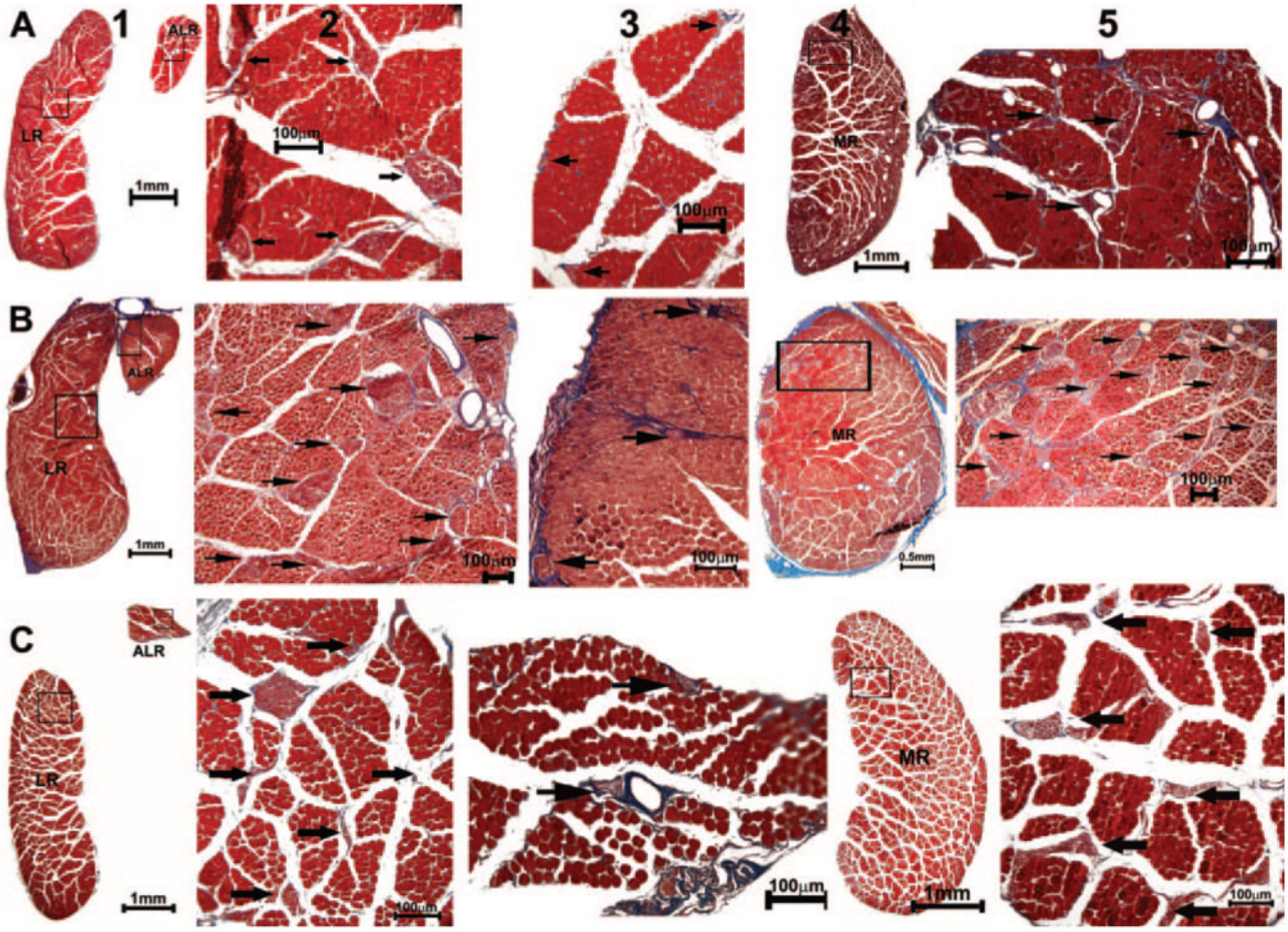

Figure 11.

Quasicoronal histologic sections from (**A**) normal (94D248 left orbit, 19.16 mm from the cornea), (**B**) naturally esotropic (124G right orbit, 23.61 mm from cornea), and (**C**) artificially esotropic (RhN4 left orbit, 20.97 mm from cornea) monkeys, stained with MT. *Columns* from *left* to *right*: LR and ALR EOMs (1) with intramuscular nerve arborization (2, 3); MR (4) and its innervation (5). *Arrows*: nerves.

Table 1

Characteristic of Animals

Monkey	Age (y)	Weight at Death (kg)	Sex	Ocular History	Visual Acuity (SVEP cyc/deg)	Pattern	Refractive Error	Strabismus Angle	Other Ocular Motor Findings
M. nemestrina									
80478	11	18.2	M	Orthotropic	Not Done	None	Not done	Ortho	None
124G	14	11.2	M	Natural infantile esotropia	OD 9.1	“A”	OD + 1.50 + 1.50 × 120°	LET 12.9°	Congenital nystagmus, latent nystagmus, pursuit and OKN asymmetry
					OS 9.5		OS + 3.00 + 1.00 × 105°		
79434	22	14.8	M	Natural infantile esotropia	OD 17.7	“A”	OD +0.50 sphere	RET 10.5°	Latent nystagmus, pursuit asymmetry, OKN asymmetry
					OS 19.3		OS +0.50 sphere		
M. mulatta									
RKb3	7	7.6	F	Orthotropic	Not Done	None	Not done	Ortho	None
94D248	8	8.0	M	Orthotropic	OD 8.6 OS 10.1	None	OD −3.00 +1.50 × 30° OS −1.50 sphere	Ortho	None
RhN4	5	7.5	M	AMO-induced infantile micro-esotropia (occlusion age 0–9 mo)	OD 15.9	“V”	OD −0.75 +2.00 × 110°	RET 4.1°	Latent nystagmus, pursuit asymmetry, OKN asymmetry
					OS 18.1		OS −0.75 +1.75 × 80°		
REd3	3	3.0	M	AMO-induced infantile micro-esotropia (occlusion age 0–9 mo)	OD 10.3	None	OD +3.00 sphere	Alternating	Latent nystagmus, pursuit asymmetry, OKN asymmetry
					OS 9.6		OS +1.25 +1.00 × 180°	5.0° ET	
RRm5	3	4.9	M	Right esotropia induced by occlusion OD (age, 3–52 wk)	OD 2.0	Unknown	OD +9.00 sphere	Ortho	Unknown (died during surgery)
					OS 13.5		OS +3.5 +1.00 × 90°		
RYu6	2	3.4	M	Prism-induced exotropia (age, 0–3 mo; 22.8° base in)	OD 21.1	“A”	OD +2.00 +1.00 × 150°	RXT 18.4°	Latent nystagmus, pursuit asymmetry, OKN asymmetry
					OS 19.1		OS +2.00 +1.00 × 40°		
M. arctoides									

Invest Ophthalmol Vis Sci. Author manuscript; available in PMC 2008 June 1.

Monkey	Age (y)	Weight at Death (kg)	Sex	Ocular History	Visual Acuity (SVEP cyc/deg)	Pattern	Refractive Error	Strabismus Angle	Other Ocular Motor Findings
IJI	6	11.0	M	Orthotropic (idiopathic adult-onset cataract, OD)	OD mature cataract OS follows	None	OD +2.50 sphere OS +2.00 sphere	Ortho	None

AMO, alternating monocular occlusion; OD, right eye; OS, left eye; OKN, optokinetic nystagmus; SVEP, sweep visual evoked potential.

Table 2

Horizontal Rectus and ALR Muscle Cross-sectional Area

Category	Monkey ID	Eye	Greater Directional Shrinkage (%)	Lesser Directional Shrinkage (%)	Cross-sectional Area*									Innervation (Axons/mm^2)		
					LR	Mean	*P* vs. Normal	MR (mm^2)	Mean	*P* vs. Normal	ALR	Mean	*P* vs. Normal	LR	MR	ALR
Normal	RKb3	R	36	43	27.1	26.0 ± 1.0	NA	23.6	22.0 ± 5.2	NA	1.1	2.4 ± 1.1	NA	*	*	3.6
	80478	R	40	50	25.2			16.1			3.0			36.5	52.7	7.0
	94D248	L	57	50	25.6			26.1			3.0			37.4	33.1	6.0
Natural esotropia	124G	L	29	31	29.3	42.4 ± 14.0	0.18	23.8	36.0 ± 11.0	0.14	8.0	6.4 ± 1.4	0.02	18.3	50.0	2.8
	79434	L	32	38	57			44.8			5.3			13.4	13.8	6.6
		R	17	29	40.9			39.7			5.8			40.2	18.4	4.3
Induced esotropia	RHn4	L	34	36	27.4	28.0 ± 1.3	0.12	25.3	28.6 ± 3.5	0.15	5.7	3.4 ± 2.1	0.52	25.0	52.9	2.4
	REd3	L	38	33	26.9			28.4			2.8			*	*	4.2
		R	47	53	29.4			32.3			1.5			*	*	8.4
Exotropia	RYu6	L	30	27	15.3	16.0 ± 1.0	0.00	11.8	13.3 ± 2.1	0.09	2.0	2.0 ± 0.0	0.67	27.9	59.5	2.4
		R	42	36	16.6			14.7			2.1			37.3	66.4	3.4

*Corrected for histologic shrinkage (mm^2).